PERGAMON

International Journal of Multiphase Flow 26 (2000) 1771–1796

International Journal of Multiphase Flow

www.elsevier.com/locate/ijmulflow

# Bubble motion in a potential flow within a Venturi

J. Soubiran, J.D. Sherwood*

*Schlumberger Cambridge Research, High Cross, Madingley Road, Cambridge CB3 0EL, UK*

Received 20 February 1999; received in revised form 25 November 1999

**Abstract**

The motion of a bubble within a liquid-filled Venturi is computed using a simple force balance which considers pressure forces, added mass, and steady drag acting on the bubble. The bubble is small compared to the pipe radius, and interactions between the bubble and the pipe wall are neglected. Interfacial tension is assumed to be sufficiently strong that the bubble remains spherical. The liquid velocity is assumed either to be a simple one-dimensional flow with velocity inversely proportional to the pipe cross-sectional area, or to be an axisymmetric potential flow. A bubble on the axis of the Venturi remains on the axis. In the absence of drag, the bubble moves through the Venturi more rapidly than the liquid. If drag is small, the model predicts that the bubble becomes trapped within the Venturi. If drag is large, relative motion between the liquid and the bubble is suppressed, and the bubble flows through the Venturi without oscillation. Off the axis, a bubble in the converging section of the Venturi accelerates towards the centreline more rapidly than the liquid. In the absence of drag, if bubbles are distributed uniformly across the cross-section of the pipe upstream of the Venturi, they will be concentrated close to the axis in the throat. The bubbles eventually cross the axis and hit the far wall of the Venturi, at which point trajectory computations were stopped. If drag acts on the bubbles, the resulting combination of oscillatory axial motion and radial motion causes the bubbles to move towards the walls of the Venturi, where the potential flow is fast and pressures are small. Order of magnitude estimates suggest that such oscillations would not be observed for air bubbles in water, since the bubbles would be deformed and drag would become large. 

*Keywords:* Bubble; Venturi; Potential flow

* Corresponding author. Tel.: +44-1223-325-363; fax: +44-1223-315-486.
*E-mail address:* sherwood@cambridge.scr.slb.com (J.D. Sherwood).

0301-9322/00/$ - see front matter 
PII: S0301-9322(99)00113-5

## 1. Introduction

The Venturi is a robust method for measuring the flow of single-phase fluid of known density at high Reynolds numbers. Multiphase flow measurement is more difficult. The density of a gas–liquid mixture depends upon the volume fraction of gas, and the velocity of gas within the Venturi is likely to differ from that of the liquid. Recent practical flow measurement devices are reviewed by Thorn et al. (1997); theoretical background is provided by Boyer and Lemonnier (1996).

The density of the gas is less than that of the liquid, and so the gas will accelerate more than the liquid in the converging section of the Venturi (Muir and Eichorn, 1963; van Wijngaarden, 1972). However, away from the centre-line the gas and liquid accelerate not only in the axial direction, but also radially. Any relative motion in the radial direction will lead to a non-uniform distribution of gas across the Venturi, and this may affect the differential pressure measured between the entrance to the Venturi and the throat. The aim of this paper is to predict trajectories of individual bubbles in an idealised Venturi. This bounded, non-uniform geometry is complex, and in order to simplify the problem the liquid velocity will be assumed either to be uniform across the pipe cross-section, or to be an irrotational potential flow. We shall neglect any changes to the liquid velocity caused by the presence of the bubble.

Previously published studies include those of Kuo and Wallis (1988), who looked at one-dimensional motion of a bubble in a slot-shaped nozzle and compared experimental results against a model which included buoyancy, steady and unsteady viscous drag, added mass (acceleration reaction) and pressure forces. Similar computations in a converging nozzle are reported by Kowe et al. (1988), who used a steady drag law. Kim and Prosperetti (1992) simulated the motion of one or more spheres in potential flow within a Venturi: they included interactions between the spheres, and between the spheres and the walls of the Venturi. The effect of gravity was investigated, but not that of drag. They noted that a sphere off the axis of the Venturi could be deflected towards the centreline and would eventually hit the far wall of the pipe. The initial motion away from the pipe wall, towards the centre-line, was also studied by Oldenziel (1979), who was concerned that this would affect the gas volume fraction in samples taken at the Venturi wall. Sherwood (2000) considered potential flow around a deforming bubble on the axis of a Venturi in the absence of drag or buoyancy forces.

We shall assume that changes in pressure as the liquid passes through the Venturi are small compared to the ambient pressure, so that variations in the bubble size may be neglected. Such variations were included in computations of cavitation bubble trajectories by Johnson and Hsieh (1966).

In Section 3, we first examine a one-dimensional model in which only the added mass and pressure forces are considered, and then discuss the effect of including a (steady) drag force. In Section 4, we consider irrotational flow of inviscid liquid through a Venturi, and compute trajectories of bubbles through the Venturi. In Section 5, we consider the effect of drag on trajectories through the Venturi.

## 2. The forces acting on the bubble

We consider an incompressible, spherical gas bubble of radius $R_0$, volume $V = \frac{4}{3}\pi R_0^3$ and density $\rho_g$ moving with velocity $\boldsymbol{v}_b$ in liquid which (in the absence of the bubble) moves with velocity $\boldsymbol{u}_l$. The liquid is incompressible with density $\rho_l$ and viscosity $\mu$. The forces acting on the bubble are discussed by Batchelor (1973) (p. 409), and Auton et al. (1988). The force due to the pressure field in the liquid in the absence of any bubble is

$$\boldsymbol{F}_p = V\rho_l \frac{D_l \boldsymbol{u}_l}{Dt} \tag{1}$$

where $D_l\boldsymbol{u}_l/Dt = \partial \boldsymbol{u}_l/\partial t + \boldsymbol{u}_l \cdot \nabla \boldsymbol{u}_l$ evaluated at the instantaneous position of the bubble. The added mass force (acceleration reaction) is

$$\boldsymbol{F}_a = C_m V \rho_l \left( \frac{D_l \boldsymbol{u}_l}{Dt} - \frac{\mathrm{d}\boldsymbol{v}_b}{\mathrm{d}t} \right). \tag{2}$$

The coefficient $C_m = \frac{1}{2}$ in unbounded fluid, but increases when the bubble is inside a liquid-filled pipe (Smythe, 1961; Cai and Wallis, 1992). We shall later assume that the bubble radius $R_0$ is small compared to a typical pipe radius $a$, so that the effect of the pipe is negligible and $C_m = \frac{1}{2}$.

We shall assume that the axis of the Venturi is vertical, as is usual in practical devices in order to avoid stratification due to buoyancy. Flow is upwards in the direction $\hat{\boldsymbol{x}}$, so that the buoyancy force on the bubble is

$$\boldsymbol{F}_b = -(\rho_g - \rho_l) V g \hat{\boldsymbol{x}} \tag{3}$$

where $g$ is the acceleration due to gravity.

Kuo and Wallis (1988) included both steady and unsteady drag forces: we shall ignore unsteady drag. The steady drag $\boldsymbol{F}_d$, reviewed by Clift et al. (1978), is sometimes written in the form

$$\boldsymbol{F}_d = \frac{1}{2} C_d \rho_l \pi R_0^2 |\boldsymbol{u}_l - \boldsymbol{v}_b| (\boldsymbol{u}_l - \boldsymbol{v}_b) \tag{4}$$

where the drag coefficient $C_d$ depends on the bubble Reynolds number

$$Re^b = \frac{2R_0 \rho_l |\boldsymbol{u}_l - \boldsymbol{v}_b|}{\mu}. \tag{5}$$

In most of the results presented here, we follow Kowe et al. (1988) and use the Levich formula for steady drag on a spherical bubble at high Reynolds number (Batchelor, 1973, p. 368)

$$\boldsymbol{F}_d = 12\pi\mu R_0 (\boldsymbol{u}_l - \boldsymbol{v}_b), \tag{6}$$

which corresponds to a drag coefficient

$$C_d = 48/Re^b. \tag{7}$$

However, the bubbles are unlikely to remain spherical when the flow rate is high. In Section 3.4 we give some order of magnitude estimates for typical velocities, and consider another force law in order to see how the choice of drag law affects the results.

The lift force due to vorticity is

$$\boldsymbol{F}_{\mathrm{lv}} = \rho_{\mathrm{l}} V C_{\mathrm{lv}} (\boldsymbol{u}_{\mathrm{l}} - \boldsymbol{v}_{\mathrm{b}}) \wedge (\nabla \wedge \boldsymbol{u}_{\mathrm{l}}) \tag{8}$$

where the lift coefficient $C_{\mathrm{lv}} = \frac{1}{2}$ in unbounded fluid. This force will be zero in the irrotational flows considered here. However, numerical computations by Magnaudet and Legendre (1998) have shown that even in the absence of vorticity a sphere is subjected to a lift force in a flow with strain rate

$$\mathsf{S} = \frac{1}{2}\left(\nabla \boldsymbol{u}_{\mathrm{l}} + (\nabla \boldsymbol{u}_{\mathrm{l}})^{\mathrm{T}}\right). \tag{9}$$

Magnaudet and Legendre propose a lift force of the form

$$\boldsymbol{F}_{\mathrm{ls}} = 2V\rho_{\mathrm{l}} C_{\mathrm{ls}} (\boldsymbol{u}_{\mathrm{l}} - \boldsymbol{v}_{\mathrm{b}}) \cdot \mathsf{T} \tag{10}$$

where

$$\mathsf{T} = \mathsf{S} - \frac{(\boldsymbol{u}_{\mathrm{l}} - \boldsymbol{v}_{\mathrm{b}}) \cdot \mathsf{S} \cdot (\boldsymbol{u}_{\mathrm{l}} - \boldsymbol{v}_{\mathrm{b}})}{|\boldsymbol{u}_{\mathrm{l}} - \boldsymbol{v}_{\mathrm{b}}|^2} \mathsf{I} \tag{11}$$

and

$$C_{\mathrm{ls}} = -1.2\left(Re^{b}\right)^{-1/3} \quad Re^{\mathrm{b}} > 100, \tag{12}$$

though in practice a bubble will no longer be spherical at sufficiently high $Re^{\mathrm{b}}$. We assume that the various forces acting on the bubble may be added linearly (e.g., Climent and Magnaudet, 1997; Hunt et al., 1997) so that the equation of motion for the bubble is

$$\rho_{\mathrm{g}} V \frac{\mathrm{d}\boldsymbol{v}_{\mathrm{b}}}{\mathrm{d}t} = \boldsymbol{F}_{\mathrm{p}} + \boldsymbol{F}_{\mathrm{a}} + \boldsymbol{F}_{\mathrm{b}} + \boldsymbol{F}_{\mathrm{d}} + \boldsymbol{F}_{\mathrm{ls}}. \tag{13}$$

We scale all velocities by $U$ (which will later be taken as the liquid velocity at the entrance to the Venturi), and all lengths by $a$, (which will later be taken as the radius of the pipe at the entrance to the Venturi). Time is scaled by $a/U$. We assume that the liquid flow is steady, with Reynolds number

$$Re = \frac{aU\rho_{\mathrm{l}}}{\mu}. \tag{14}$$

The equation of motion for the bubble (13) becomes

$$\frac{\mathrm{d}\boldsymbol{v}_{\mathrm{b}}}{\mathrm{d}t} = M_{\mathrm{a}} \boldsymbol{u}_{\mathrm{l}} \cdot \nabla \boldsymbol{u}_{\mathrm{l}} - M_{\mathrm{b}} Fr\, \hat{\boldsymbol{x}} - M_{\mathrm{d}} (\boldsymbol{v}_{\mathrm{b}} - \boldsymbol{u}_{\mathrm{l}}) + M_{\mathrm{ls}} (\boldsymbol{v}_{\mathrm{b}} - \boldsymbol{u}_{\mathrm{l}}) \cdot \mathsf{T} \tag{15}$$

where

$$Fr = \frac{ga}{U^2} \tag{16}$$

is a Froude number, and the other coefficients are

$$M_a = \frac{\rho_l(1+C_m)}{\rho_g+\rho_l C_m}, \quad M_b = \frac{\rho_g-\rho_l}{\rho_g+\rho_l C_m}, \quad M_d = \frac{9\rho_l}{(\rho_g+\rho_l C_m)ReR_0^2}, \quad M_{ls} = \frac{-2\rho_l C_{ls}}{\rho_g+\rho_l C_m}. \tag{17}$$

Note that the bubble radius $R_0$ which appears in the expression for $M_d$ has been non-dimensionalised by $a$. We now set the gas density $\rho_g = 0$ and take $C_m = \frac{1}{2}$, so that

$$M_a = 3, \quad M_b = -2, \quad M_d = \frac{18}{ReR_0^2}, \quad M_{ls} = \frac{4.8}{(Re^b)^{1/3}}. \tag{18}$$

In the results to be presented here we set $Fr = 0$, so that the effects of gravity are neglected. Similarly, the lift force $\boldsymbol{F}_{ls}$ will be set to zero, except in Section 5.2 where it will be shown that the effect of $\boldsymbol{F}_{ls}$ is typically small. Thus, we shall investigate how trajectories depend upon $M_d$, the ratio of drag to inertia.

## 3. A simple one-dimensional model with drag

### 3.1. The Venturi geometry

Fig. 1 shows an axisymmetric Venturi with inlet diameter $2a$: we non-dimensionalise all lengths by $a$. The pipe is cylindrical, with radius

$$R_p = \begin{cases} 1 & 0 < x < x_1 \\ 1 - \dfrac{(x-x_1)(1-\beta)}{x_2-x_1} & x_1 < x < x_2 \\ \beta & x_2 < x < x_3 \\ 1 - \dfrac{(x_4-x)(1-\beta)}{x_4-x_3} & x_3 < x < x_4 \\ 1 & x_4 < x < x_5, \end{cases} \tag{19}$$

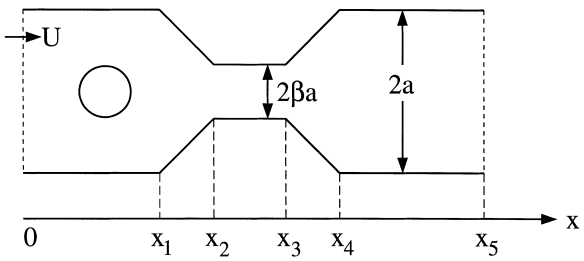


Fig. 1. A bubble at $x = x_b$ in a Venturi.

where $\beta$ is the non-dimensional radius of the Venturi throat and $x$ the distance along the axis. In all the work presented here we shall assume that $\beta = \frac{1}{2}$, $x_1 = 3.0$, $x_2 = 5.7$, $x_3 = 6.7$, $x_4 = 10.5$. This corresponds to an ISO standard Venturi (British Standards Institution, 1997) with a $21^\circ$ converging section and $15^\circ$ diverging section. The diverging section is longer than the converging one in order to reduce separation and hence total pressure loss, but separation will not be completely eliminated. We shall ignore separation: results obtained for an even longer diverging section (in which effects of separation should be reduced even further) are qualitatively similar to those presented here.

### 3.2. Uniform velocity across cross-section: Levich drag

In this section, we follow Kuo and Wallis (1988), Kowe et al. (1988) and Sherwood (2000) and consider a one-dimensional model for the motion of the bubble. Like Kowe et al. we assume that the fluid velocity is uniform across the cross-section. We non-dimensionalise all velocities by the velocity $U$ at the entrance, so that the dimensionless liquid velocity is

$$u_\mathrm{l} = R_\mathrm{p}^{-2}. \tag{20}$$

Time is non-dimensionalised by $a/U$, densities by $\rho_\mathrm{l}$ and pressures by $\rho_\mathrm{l} U^2$.

The lift force is identically zero and we neglect buoyancy, so that the governing equation for the motion of the bubble centre $x_\mathrm{b}(t)$ becomes

$$\frac{\mathrm{d}^2 x_\mathrm{b}}{\mathrm{d}t^2} = 3u_\mathrm{l}\frac{\mathrm{d}u_\mathrm{l}}{\mathrm{d}x} - M_d\left(\frac{\mathrm{d}x_\mathrm{b}}{\mathrm{d}t} - u_\mathrm{l}\right). \tag{21}$$

We assume that upstream of the Venturi the bubble moves at the same velocity as the liquid, and we take as initial conditions

$$x_\mathrm{b} = 1, \qquad v_\mathrm{b} = \frac{\mathrm{d}x_\mathrm{b}}{\mathrm{d}t} = 1 \quad \text{at } t = 0. \tag{22}$$

In the limit $Re \to \infty$, drag can be neglected and Eq. (21) may be integrated:

$$v_\mathrm{b}^2 = \left(\frac{\mathrm{d}x_\mathrm{b}}{\mathrm{d}t}\right)^2 = 3u_\mathrm{l}^2 - 2, \tag{23}$$

a particular case of a result given by Kowe et al. (1988) (Eq. 31 of the reference). In the throat of the Venturi, if $\beta = \frac{1}{2}$ then $u_\mathrm{l} = 4$ and $v_\mathrm{b} = 6.78$. Sherwood (2000) compares the prediction (23) with numerical computations of potential flow around a bubble on the axis of a Venturi, and discusses the approximation of uniform flow (20) and the approximation of the added mass coefficient by its value $C_\mathrm{m} = \frac{1}{2}$ in unbounded flow.

The velocity (23) is shown as a function of position in curve (a) of Fig. 2. The deceleration of the bubble in the diverging section of the Venturi is equal to the acceleration in the converging section, so that the bubble emerges from the Venturi with the same velocity as the liquid. The bubble moves faster than the liquid in the throat, so that if a small amount of drag is introduced the bubble slows down. After decelerating in the diverging section, the bubble

emerges from the Venturi moving more slowly than the liquid. It subsequently speeds up, due to drag, and regains the velocity of the liquid. This is shown in curve (b) of Fig. 2 for the case $M_d = 0.056$.

If drag is increased even more, the velocity at the end of the throat is sufficiently small such that the adverse pressure gradient in the diverging section brings the bubble to a halt and then reverses its velocity. Oscillations are predicted, as shown in Figs. 3 and 4. Increasing the drag further increases the rate of decay of the oscillations and at $M_d = 2.92$ (Fig. 5) the oscillations are heavily damped. Similar oscillatory behaviour has been previously observed in computations by van Wijngaarden (private communication).

If drag is large, the bubble moves with the liquid, so that $v_b \approx u_l$ and no oscillations occur. The damped oscillations of Fig. 5 disappear if $M_d$ is increased to 2.93, as shown in curve (c) of Fig. 2.

A steady solution of Eq. (21) with the bubble at a fixed position $x_b$ is possible if

$$\frac{du_l}{dx} = -\frac{M_d}{3} \tag{24}$$

i.e. if

$$\frac{1}{R_p^3}\frac{dR_p}{dx} = \frac{M_d}{6}. \tag{25}$$

The left-hand side of Eq. (25) takes its maximum value $\beta^{-3}(1-\beta)/(x_4 - x_3)$ at the start of the diverging section. The minimum value, at the end of the diverging section, is $(1-\beta)/(x_4 - x_3)$.

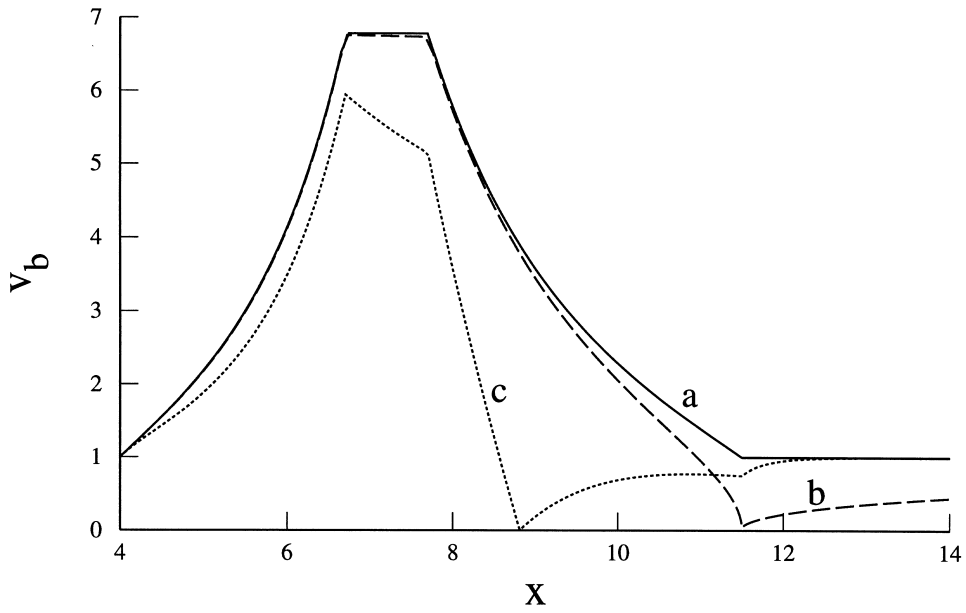


Fig. 2. The velocity $v_b$ of the bubble as a function of position $x$. (a) $M_d = 0$; (b) $M_d = 0.056$; (c) $M_d = 2.93$.

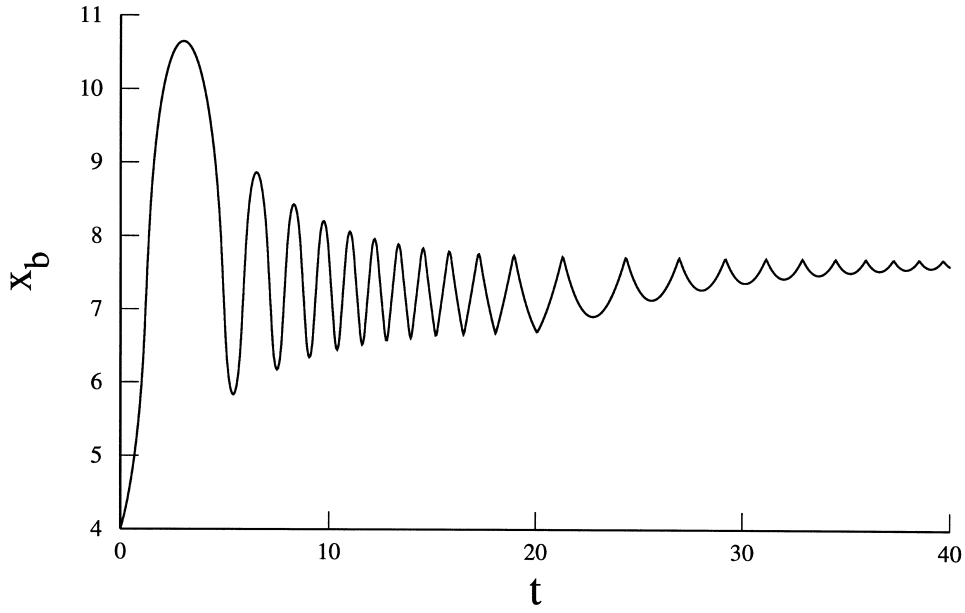


Fig. 3. The position $x_b$ of the bubble as a function of $t$. $M_d = 0.18$.

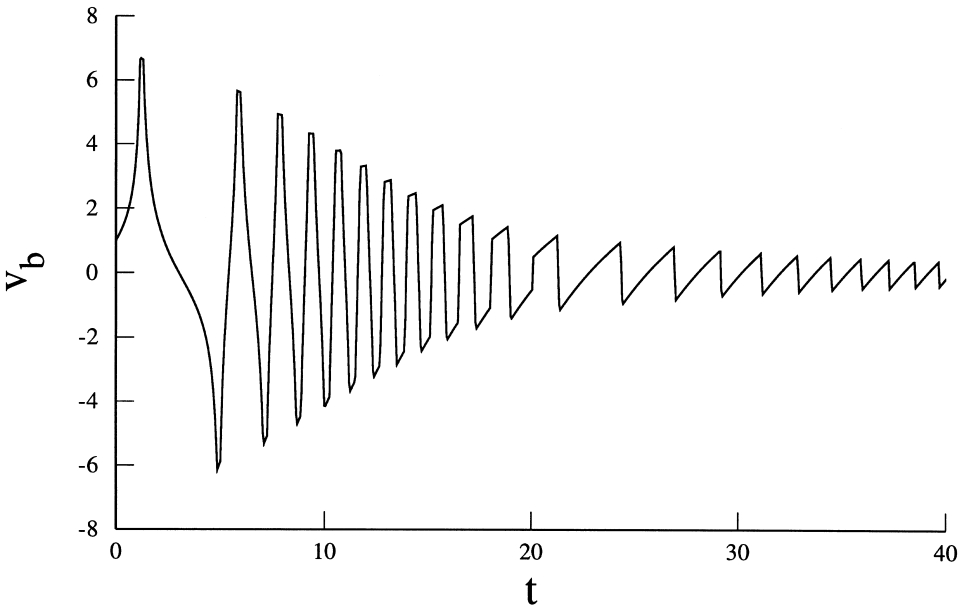


Fig. 4. The velocity $v_b$ of the bubble corresponding to the results of Fig. 3.

Thus, when $\beta = \frac{1}{2}$ and $x_4 - x_3 = 3.8$, a steady solution might be possible over the range

$$0.79 < M_d < 6.3. \tag{26}$$

No steady solution is possible within the converging or straight sections of the pipe.

We now consider a bubble which oscillates close to the end of the throat of the Venturi. We assume that the bubble velocity is small, so that $dx_b/dt$ may be neglected on the right-hand side of Eq. (21). We take a local coordinate $y = x - x_3$ measured from the end of the throat, so that Eq. (21) becomes

$$\frac{d^2 y_b}{dt^2} = 3u_l \frac{du_l}{dy} + M_d\left(u_0 + \frac{du_l}{dy} y_b + \cdots\right), \tag{27}$$

where $u_0$ is the liquid velocity at $y = 0$ and $y_b = x_b - x_3$ is the position of the bubble. This integrates to give

$$\frac{1}{2}\left(\frac{dy_b}{dt}\right)^2 = \frac{3}{2}u_l^2 + M_d\left[u_0 y_b + \left(\frac{du_l}{dy}\right)\frac{y_b^2}{2} + \cdots\right] + C, \tag{28}$$

where $C$ is a constant of integration. We now expand $u_l^2$, so that the governing equation becomes

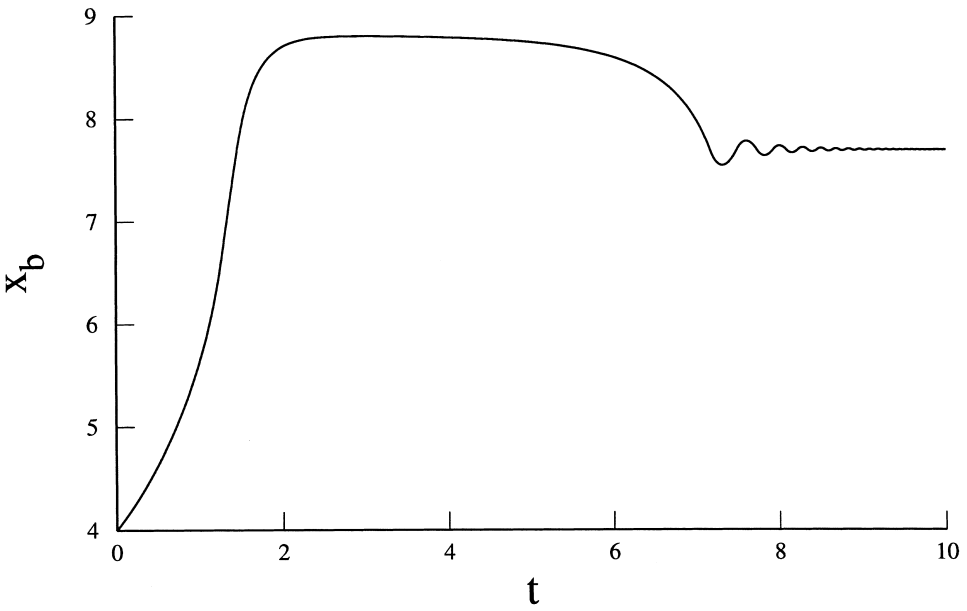


Fig. 5. The position $x_b$ of the bubble as a function of time $t$. $M_d = 2.92$.

$$\left(\frac{\mathrm{d}y_\mathrm{b}}{\mathrm{d}t}\right)^2 = 3u_0^2 + u_0 y_\mathrm{b}\left(6\frac{\mathrm{d}u_\mathrm{l}}{\mathrm{d}y} + 2M_\mathrm{d}\right) + \cdots + C, \tag{29}$$

where we have neglected terms $O(y_\mathrm{b}^2)$. Now

$$u_0 = \beta^{-2} \quad y = 0 \tag{30}$$

and

$$\frac{\mathrm{d}u_\mathrm{l}}{\mathrm{d}y} = -\frac{2}{R_\mathrm{p}^3}\frac{\mathrm{d}R_\mathrm{p}}{\mathrm{d}y} = 0 \qquad y = 0^- \tag{31a}$$

$$\frac{\mathrm{d}u_\mathrm{l}}{\mathrm{d}y} = -\frac{2}{R_\mathrm{p}^3}\frac{\mathrm{d}R_\mathrm{p}}{\mathrm{d}y} = \frac{2(1-\beta)}{\beta^3(x_4 - x_3)} \quad y = 0^+. \tag{31b}$$

If an oscillation about $y = 0$ occurs, $\mathrm{d}y_\mathrm{b}/\mathrm{d}t = 0$ at some point in both $y < 0$ and $y > 0$, and by Eq. (29) the latter requires

$$\frac{6(1-\beta)}{\beta^3(x_4 - x_3)} > M_\mathrm{d}, \tag{32}$$

so that if $\beta = \frac{1}{2}$, then $M_\mathrm{d} < 6.3$ is a necessary (but not sufficient) criterion for oscillation. The assumption that $|\mathrm{d}x_\mathrm{b}/\mathrm{d}t|$ can be neglected compared to $u_\mathrm{l}$ in Eq. (21) is satisfied at the turning points of the oscillation, but is not necessarily satisfied at intermediate points during the early stages of oscillation, as can be seen in Fig. 4. Similarly, the expansion of $u_\mathrm{l}$ and subsequent neglect of terms $O(y_\mathrm{b}^2)$ will be a poor approximation initially, when the oscillations are large. However, if a bubble is trapped the approximations made above become increasingly accurate as the oscillations decay (Figs. 3 and 4). Full numerical solutions of Eq. (21) with $u_\mathrm{l} = R_\mathrm{p}^{-2}$ predict that a bubble with upstream velocity $v_\mathrm{b} = 1$ is trapped by oscillations if $0.0561 < M_\mathrm{d} < 2.92$.

At the sharp corners of the Venturi the pipe radius $R_p$ is continuous, but the derivative $\mathrm{d}R_p/\mathrm{d}x$ is not. Consequently $u_\mathrm{l} = R_p^{-2}$ has discontinuous derivatives at $x_2$ and $x_3$, so that the pressure and added mass forces acting on the bubble are discontinuous at these points. This is clearly seen in the computed bubble velocity $v_\mathrm{b}$ shown in Fig. 4.

Such oscillations have not (to our knowledge) been observed experimentally, and we should therefore ask ourselves the reason for this. One obvious problem with the model presented above is the lack of separation downstream of the Venturi throat. Such separation will reduce the adverse pressure gradient within the diverging section. The sensitivity of the model to this effect can be tested by setting $x_4 = 14.9$, which corresponds to an ISO Venturi with a $7^\circ$ diverging section. Oscillations are again predicted by the model over the range $0.0039 < M_\mathrm{d} < 0.98$.

The inclusion of a small amount of buoyancy, directed along the axis of the vertically oriented Venturi, changes the values of $M_\mathrm{d}$ for which oscillation occurs, but does not qualitatively affect the results. We show below (Sections 3.3 and 5.1) that oscillations are predicted for a more realistic velocity $u_\mathrm{l}$ with continuous derivatives. In Section 3.4, we

consider deformation of the bubble and consequent modification of the drag law. This turns out to be a possible explanation for the absence of observed bubble oscillations.

### 3.3. A liquid velocity with continuous derivatives

The simple one-dimensional model of Section 3.2 uses a liquid velocity $u_l$ with a discontinuous derivative. We shall see in Section 4.1 (Fig. 6) that the potential flow velocity along the centreline of the Venturi is smooth. It is straightforward to repeat the one-dimensional analysis of Section 3.2, using a liquid velocity

$$u_l = a_0 - a_2 X^2, \tag{33}$$

where $X = x - x_m$ is an axial coordinate measured from the position $x_m$ at which $u_l$ is greatest.

The equation of motion (21) for the bubble at $X_b = x_b - x_m$ is

$$\frac{d^2 X_b}{dt^2} = -6a_2 X_b\left(a_0 - a_2 X_b^2\right) - M_d\left(\frac{dX_b}{dt} - a_0 + a_2 X_b^2\right). \tag{34}$$

We assume that $a_2 X_b^2 \ll a_0$ so that Eq. (34) becomes

$$\frac{d^2 X_b}{dt^2} + M_d \frac{dX_b}{dt} + 6a_0 a_2 X_b = M_d a_0. \tag{35}$$

A steady solution of Eq. (35) is possible at $X_b = M_d/(6a_2)$ and if $M_d^2 \ll 36a_0 a_2$ the neglected quadratic term in Eq. (34) is small, with $a_2 X_b^2 \ll a_0$. There are also solutions of Eq. (35) of the form

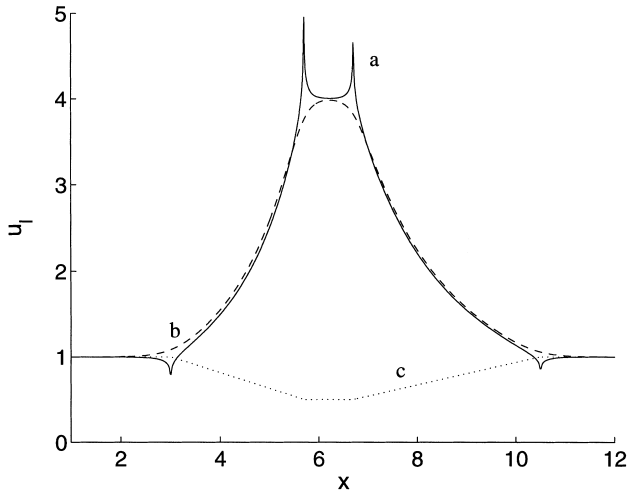


Fig. 6. The non-dimensional liquid velocity $|u_l|$ (a) at the wall; (b) along the centreline. (c) The shape of the Venturi.

$$X_b(t) = \frac{M_d}{6a_2} + e^{\sigma t} \tag{36}$$

with

$$\sigma = -\frac{1}{2}M_d \pm \frac{1}{2}\left(M_d^2 - 24a_0a_2\right)^{1/2}. \tag{37}$$

The solution $X_b(t)$ of the linearised equation (35) oscillates when $M_d < (24a_0a_2)^{1/2}$ and $Re(\sigma) = -\frac{1}{2}M_d$, so that the rate of damping increases with $M_d$.

### 3.4. An alternative drag law

We now question the validity of the simple Levich drag law (7) and in the following order of magnitude estimates we use a tilde to denote a dimensional quantity. If we assume a liquid flow rate of 10 $m^3\ h^{-1}$ in a pipe of radius $\tilde{a} = 25$ mm, the liquid velocity at the entrance to the Venturi is $\tilde{U} = 1.4\ m\ s^{-1}$. Taking the liquid to be water with viscosity $\tilde{\mu} = 10^{-3}$ Pa s and density $\tilde{\rho}_l = 10^3\ kg\ m^{-3}$ leads to a pipe Reynolds number $Re = 3.5 \times 10^4$. The range $0.0561 < M_d < 2.92$ corresponds to a range of non-dimensional bubble sizes $0.01 < R_0 < 0.1$. In the absence of drag, the maximum non-dimensional velocity of the bubble relative to the liquid is $v_b - u_l = 2.78$. We assume an interfacial tension $\tilde{\gamma} = 80\ mN\ m^{-1}$ and we non-dimensionalise this by $\tilde{\rho}_l\tilde{U}^2\tilde{a}$ to obtain a non-dimensional interfacial tension $\gamma = 1.6 \times 10^{-3}$. Hence, the Weber number for a bubble of radius $R_0 = 0.01$ is $We = 2R_0(v_b - u_l)^2/\gamma \approx 100$. We conclude that the bubble will not remain spherical (Moore, 1965).

It is far from clear whether the bubble will survive intact, but we assume that it does and in the absence of any information concerning the bubble shape we adopt the drag coefficient $C_d = \frac{8}{3}$ corresponding to a highly deformed, spherical cap bubble (Clift et al., 1978). If nothing else, this will at least indicate the sensitivity of the predictions to the choice of drag law. The added mass of the bubble can be made arbitrarily large if the bubble is deformed into a sufficiently thin flat disc, but we shall keep $C_m = \frac{1}{2}$ in order to investigate the effect of changing the drag law alone. Lift forces on a non-spherical bubble will in practice become important, but we shall ignore these, again in order to investigate drag alone. The equation of motion for the bubble is still given by Eq. (15), but with $M_d = 2|u_l - v_b|/R_0$. Oscillations are obtained over the range $1.7 < R_0 < 71$ but we dismiss these unphysical results since the bubbles are larger than the pipe itself. Thus, once the bubble has deformed the drag will be larger than that predicted by the Levich law (7) and may be too large for oscillations to occur. In the absence of precise information about bubble shape it is difficult to pursue the analysis in more detail, but it seems likely that the oscillations predicted here would not be observed with gas bubbles in water.

In Section 5.2, we show that even if we could find a fluid for which the interfacial tension is sufficiently strong that the bubble remains spherical, the oscillations predicted using the Levich law are unlikely to be observed since motion along the centre-line is unstable. Bubbles move away from the centre-line towards points of low pressure at the walls of the Venturi.

## 4. Radial motion of bubbles within a Venturi

### 4.1. The velocity field within the Venturi

Gas bubbles flowing in a fluid-filled circular pipe are unlikely to be distributed uniformly over the pipe cross-section, even when the pipe is vertical. There is experimental evidence (Lance and Lopez de Bertodano, 1994; Lopez de Bertodano et al., 1994; Serizawa and Kataoka, 1994) that bubbles accumulate at the wall when the flow is turbulent, though at high gas cut (and high flow rate) we expect a transition to annular flow, in which a film of liquid covers the pipe walls and the gas is concentrated in the centre of the pipe. If the gas–liquid mixture is inhomogeneous, the pressure distribution in a Venturi will differ from that within a homogeneous fluid, and hence, the differential pressure from the entrance to the throat will also be modified.

Here we consider how the radial distribution of gas bubbles is modified on passing through a Venturi. Full potential flow computations of a deformable bubble moving along the centreline of a Venturi indicate that in the absence of drag, the one-dimensional model of Section 3 predicts the bubble motion if the bubble remains spherical and $R_0 \ll 1$ so that $C_m = \frac{1}{2}$. We now consider the trajectories of bubbles which lie off the axis. In order to compute bubble trajectories within the Venturi by means of Eq. (15), we require the liquid velocity field $\boldsymbol{u}_l(x, r) = (u_x, u_r, u_\theta)$ where $(x, r, \theta)$ are cylindrical coordinates. We assume $u_\theta = 0$ so that each trajectory remains in a plane corresponding to constant $\theta = \theta_0$ (or $\theta = \theta_0 + \pi$ if the bubble crosses the axis of the pipe). Later figures will show trajectories in one such plane, described by Cartesian coordinates $(x, y)$. We shall assume $\boldsymbol{u}_l = (u_x, u_r)$ to be potential flow. This neglects turbulence, and neglects the effect of viscosity on the liquid velocity $\boldsymbol{u}_l$ even though the effects of viscous drag on the bubble will be included in the trajectory computations. However, this choice is sufficiently simple to allow our attention to be focussed on the motion of the bubbles, rather than on the computation of a more realistic liquid velocity field.

The irrotational fluid velocity $\boldsymbol{u}_l$ can expressed as

$$\boldsymbol{u}_l = \nabla \Phi \tag{38}$$

where the potential $\Phi$ satisfies

$$\nabla^2 \Phi = 0. \tag{39}$$

The solution of the Laplace equation (39) can be obtained by means of a boundary integral technique described by e.g. Jaswon and Symm (1977). If $\tilde{\Phi}$ and $\Phi$ are solutions of the Laplace equation within a domain $\Omega$ with boundary $S$, then

$$\int_\Omega \left(\Phi \nabla^2 \tilde{\Phi} - \tilde{\Phi} \nabla^2 \Phi\right) \mathrm{d}\Omega = \int_S \left(\Phi \frac{\partial \tilde{\Phi}}{\partial n} - \tilde{\Phi} \frac{\partial \Phi}{\partial n}\right) \mathrm{d}S, \tag{40}$$

where $\boldsymbol{n}$ is the outward facing normal to the boundary $S$. If we take $\tilde{\Phi}$ to be the fundamental singularity, then

$$c\Phi(x,r) = \int_S \left( \tilde{\Phi}(x',r';x,r)\frac{\partial \Phi(x',r')}{\partial n} - \Phi(x',r')\frac{\partial \tilde{\Phi}(x',r';x,r)}{\partial n} \right) \mathrm{d}S_{x'} \tag{41}$$

where $c = 1$ for all points within $\Omega$, $c = \frac{1}{2}$ on smooth boundaries and $c = \frac{1}{4}$ at boundary corners with interior angle $\pi/2$. We assume that the inlet and outlet to the pipe are sufficiently far from the Venturi such that the flow is close to uniform, with $|\boldsymbol{n}\cdot\nabla\Phi| = U$. On the walls of the pipe $\boldsymbol{n}\cdot\nabla\Phi = 0$. Thus, we have a Neumann problem and $\Phi$ can be found on the boundary $S$ by solving the integral equation (41), with angular integration over the surface $S$ performed analytically. Once $\Phi$ is known over the boundary, then $\Phi$ can be obtained within the interior of $\Omega$ by evaluating the integral (41): this requires first derivatives of the Green's function $\tilde{\Phi}$. To obtain the velocity field $\boldsymbol{u} = \nabla\Phi$, we therefore require second derivatives of $\tilde{\Phi}$, and to obtain the gradient of the velocity field required to evaluate the added mass $\boldsymbol{F}_a$ (2), we need third derivatives of $\tilde{\Phi}$. The angular integration of these derivatives entails considerable algebra.

We take the simple Venturi of Section 3.1 with $\beta = \frac{1}{2}$ and total length $x_5 = 13.5$. The entrance and exit to the pipe were discretised as 21 points spaced equally over [0, 1]. The pipe wall was represented by 901 points interpolated by splines. This interpolation had the effect of rounding the corners of the converging, throat and diverging sections of the Venturi, thereby avoiding singularities in the solution of the Laplace equation (39). Fig. 6 shows the liquid velocity along the centreline of the pipe and at the wall as a function of the axial position. The wall velocity is large, but finite, at the rounded corners at the beginning and end of the throat.

The total volumetric flow rate

$$q_l(x) = 2\pi \int_0^{R_p} r u_x(x,r)\,\mathrm{d}r \tag{42}$$

across the pipe cross-section should be equal to $\pi$ at all axial positions $x$, and this was used to

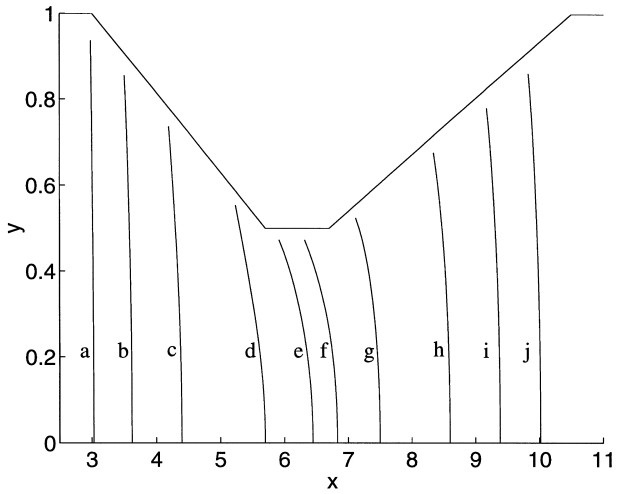


Fig. 7. The position of marked fluid particles, initially at $x = 1$ at time $t = 0$, at times: (a) $t = 2.0$; (b) $t = 2.5$; (c) $t = 3.0$; (d) $t = 3.5$; (e) $t = 3.7$; (f) $t = 3.8$; (g) $t = 4.0$; (h) $t = 4.5$; (i) $t = 5.0$; (j) $t = 5.5$.

check the accuracy of the scheme. Errors in $q_l$ were at most 0.6% and were greatest at the beginning and end of the throat, where wall velocities are large. More generally, numerical problems due to the finite discretisation of the boundary were encountered when computing velocities close to the walls of the pipe. When the representation of the boundary was refined such problems were reduced, and for the discretisation used here were restricted to a region $r > 0.98R_p$.

Fig. 7 shows the motion of a line of marked fluid particles, initially at $x = 1$ at time $t = 0$. Fluid particles near the wall are held up by the corners at the entrance and exit to the Venturi, but speed up at the entrance and exit to the throat. Even so, the net result is that such particles take longer to pass through the Venturi than those on the centreline. By starting the computations at $x = 1$, rather than at $x = 0$, we avoid any inaccuracies in the computed velocity field close to the boundary of the flow domain. The figure shows half of the pipe, with the Venturi centreline along the $x$-axis.

### 4.2. Motion of a bubble in the absence of drag

Having obtained a representation for the liquid velocity $\boldsymbol{u}_l$ within the Venturi, we may determine the trajectories of bubbles which initially lie off the axis. Eq. (15) was integrated by means of the NAG routine D02CJF (a variable step Adams method). Throughout Section 4 we assume that viscosity is negligibly small, so that we set $M_d = M_{ls} = 0$ and neglect both drag and lift. Since we neglect interactions between the bubble and the walls of the pipe, we assume not only that the bubble radius $R_0$ is small compared to the pipe radius $R_p$, as in Section 3, but also that $R_0$ is small compared to the distance of the bubble from the wall.

In general, we followed trajectories from $x_0 = 1$ until the bubble reached the outlet of the pipe. However, problems were encountered when the bubble was near either the pipe wall or the axis of the pipe. Although no difficulty was encountered on the axis itself, numerical evaluation of the liquid velocity was poor at radial positions $0 < r < 10^{-4}$ and it was no longer possible to integrate the differential equations for the bubble trajectories in this region. This problem was avoided by a simple extrapolation of the trajectory across the axis.

If a bubble hits the pipe wall we need a physical understanding of its subsequent behaviour. Although bubbles have been observed to bounce at solid walls when the liquid is at rest (Tsao and Koch, 1997), in a real Venturi there will be a viscous boundary layer, within which bubbles may be trapped by lift forces (8) which are absent in the irrotational flows considered here. We chose to stop the computation of any trajectory at the point where it reaches the pipe wall. This has implications for the conservation of bubbles. However, it will be shown later (Fig. 11) that bubbles hit the pipe wall only downstream of the throat and the fraction of bubbles removed by such impacts remains small.

Fig. 8 shows the trajectories of bubbles which start at various initial radial positions $r_0$. The figure shows a plane $(x, y)$ cross-section on which lics the centreline $y = 0$ of the Venturi. Only trajectories which start in $y \geq 0$ are shown. If a bubble starts on the axis of the Venturi it remains on the axis, but in general bubbles do not follow the liquid stream-lines. At the start of the converging section of the Venturi the liquid accelerates inwards towards the axis, and the bubbles, which have only half the inertia of the liquid they replace, accelerate more rapidly. At the end of the converging section, the radial velocity of the liquid decreases in magnitude

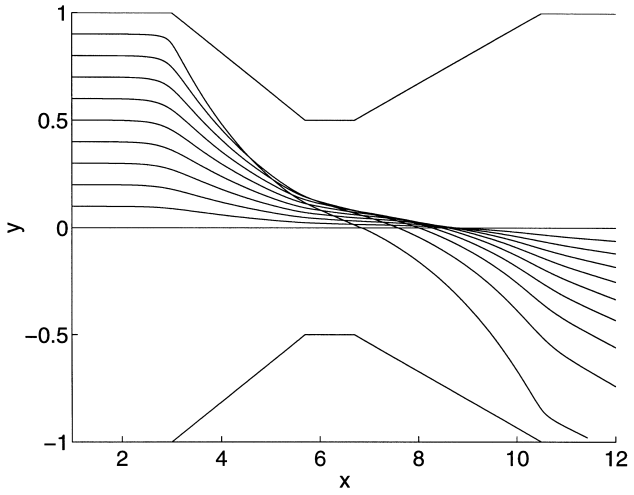


Fig. 8. Trajectories of bubbles passing through a Venturi. The only forces acting on the bubbles are dynamical pressure and added mass forces.

and returns ultimately to zero. However, although the radial velocity of the bubbles decreases, it does not become zero. The bubbles eventually cross the pipe axis and hit the opposite wall. We see from Fig. 9 that the further a bubble is initially from the axis of the pipe, the more rapidly it is accelerated towards the centre of the pipe and towards the opposite wall. At the throat of the Venturi, the bubbles are concentrated in the centre of the pipe ($r \leq 0.2$). A maximum in gas volume fraction close to the axis in the throat has been observed

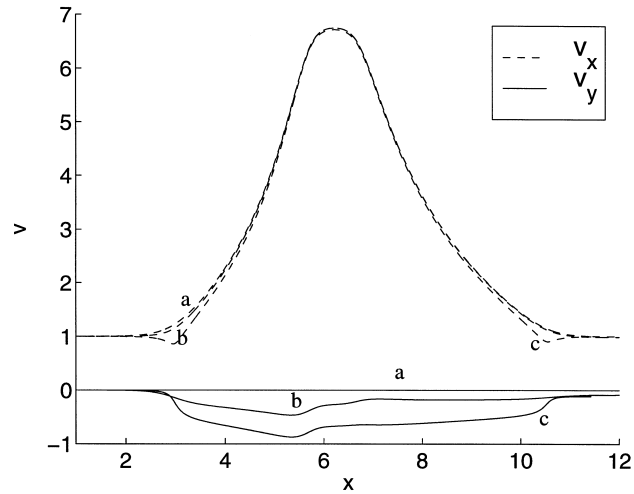


Fig. 9. Axial velocity $v_x$ - - - -, and transverse velocity $v_y$ ——— of bubbles flowing through the Venturi from three different initial radial positions: (a) $r_0 = 0$; (b) $r_0 = 0.5$; (c) $r_0 = 0.9$.

experimentally by Thang and Davis (1979), and similar computations of trajectories which cross the axis have been reported by Kim and Prosperetti (1992).

Fig. 9 shows the velocity components ($v_x$, $v_y$) of a bubble as it flows through the Venturi. The axial velocity $v_x$ is maximum in the centre of the throat, but does not depend strongly on the initial radial position $r_0$. The transverse velocity $v_y$, however, depends strongly on $r_0$.

### 4.3. The radial distribution of bubbles

We assume that there are no interactions between bubbles, so that the evolution of bubble volume fraction as a function of axial position may be determined by computing the trajectories of individual bubbles. We write the gas volume fraction $\alpha_g$ in the form

$$\alpha_g(x, r) = \alpha_0 P(x, r). \tag{43}$$

In the computations presented here, we assume that upstream of the Venturi, at $x_0$, the volume fraction $\alpha_g = \alpha_0$ is uniform across the pipe, so that

$$P(x_0, r) = 1. \tag{44}$$

However, it would be straightforward to determine the evolution of more complicated, non-uniform upstream gas volume fractions.

If a bubble which starts at ($r_0$, $x_0$) passes through ($x$, $r_1$), we may represent this trajectory by a function

$$g(r_0; x) = r_1. \tag{45}$$

Bubble trajectories starting at various radial positions $r_0$ were computed, and intermediate

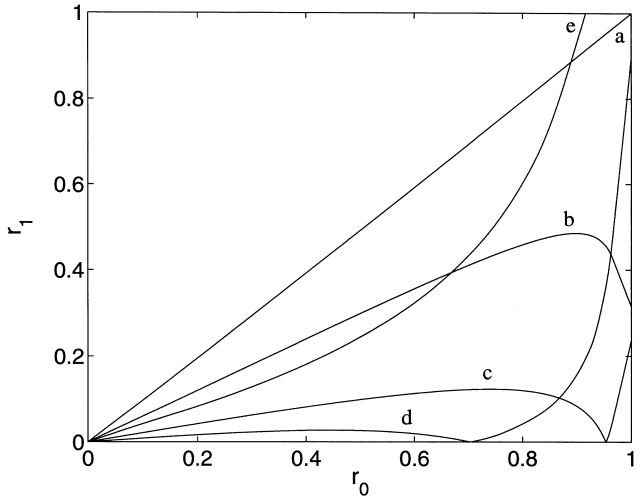


Fig. 10. Radial position $r_1 = g(r_0)$ of the bubble as a function of the initial position $r_0$, at various axial positions $x$. (a) $x = 2.5$; (b) $x = 4$; (c) $x = 6$; (d) $x = 8$; (e) $x = 11$.

values of $g$ were interpolated by means of cubic splines. Typical results for $g$ are shown in Fig. 10. Note that when $x > 3.8$, the function $g(r_0)$ is no longer monotonic. Wherever trajectories intersect one another, the inverse function $g^{-1}(x, r_1) = r_0$ is multiple valued. In Fig. 8, we see points at which two trajectories intersect. However, there are also trajectories, in the plane of the figure but not shown, which start at $y_0 < 0$. Thus, $g^{-1}$ can take up to three values. If bubbles had been allowed to re-bound from the walls, the function $g^{-1}$ would have been even more complicated. Sufficiently far downstream almost all trajectories have crossed the centre-line, as seen in curve (e) of Fig. 10.

We now seek an equation for the evolution of $P(x, r_1)$. Since the bubbles are assumed incompressible, in steady state the volume flux of bubbles

$$q_g = 2\pi \int_0^{R_p} r_1 \alpha_g(x, r_1) v_x(x, r_1)\, dr_1 \tag{46}$$

is independent of $x$, with $q_g = \pi\alpha_0$ since we have assumed $P(x_0,\ r_0) = v_x(x_0,\ r_0) = 1$. More specifically, we may consider bubble trajectories which start in the range $(r_0, r_0 + \delta r_0)$ at $x = x_0$, and are to be found in the range $(r_1, r_1 + \delta r_1)$ at $x$. Then,

$$r_1 + \delta r_1 = g(r_0, x_1) + \frac{\partial g}{\partial r_0}\delta r_0. \tag{47}$$

If we assume for the moment that all the bubbles in $(r_1, r_1 + \delta r_1)$ come from $(r_0, r_0 + \delta r_0)$, then by conservation of bubble flux

$$r_0 \alpha_g(x_0, r_0) v_x(x_0, r_0) \delta r_0 = r_1 \alpha_g(x, r_1) v_x(x, r_1) |\delta r_1| \tag{48}$$

where we have to take $|\delta r_1|$ in Eq. (48) since $r_1$ may be a decreasing function of $r_0$ at the point in question. Hence, by Eqs. (47) and (48)

$$\alpha_g = \alpha_0 P(x, r_1) = \frac{\alpha_0 P(x_0, r_0) r_0 v_x(x_0, r_0)}{g(r_0, x)\left|\frac{\partial g}{\partial r_0}\right| v_x(x, r_1)}. \tag{49}$$

More generally, since $g^{-1}$ is many-valued there can be several trajectories, starting at different $r_0$, which pass through the same point at $(x, r_1)$. Their contributions to $\alpha_g$ at $x$ will be additive. We have already seen in Fig. 9 that bubbles hit the walls of the Venturi and, as explained above, trajectory calculations were not continued beyond the point of impact. The larger the initial radial position $r_0$ of the bubble, the smaller the value of $x$ at which impact occurs. We may determine the initial radial position $r_0^1$ of the bubble which impacts the wall at any given point $x$ by solving

$$r_0^1(x) = g^{-1}\big(x, R_p\big). \tag{50}$$

The volume flux of bubbles which has been lost (through wall impact) at an axial position $x$ is

$$q_g^{\text{lost}}(x) = 2\pi \int_{r_0^1(x)}^{R_p(x_0)} r \alpha_g(x_0, r) v_x(x_0, r)\, dr = \alpha_0 \pi \Big[1 - \big(r_0^1(x)\big)^2\Big]. \tag{51}$$

Fig. 11 shows $q_g^{lost}/\alpha_0\pi$ as a function of the axial position $x$. Bubbles begin to hit the walls at $x = 7.3$, downstream of the end of the Venturi throat ($x_3 = 6.7$), and $q_g^{lost}$ increases thereafter approximately linearly with $x$.

In Fig. 8 we can see a region close to the wall of the Venturi that is devoid of bubbles. This is separated from the region containing bubbles by the envelope of the trajectories. This envelope corresponds to the maximum in $g(r_0, x)$ which can be seen in Fig. 10. We define $r_f(x)$ to be the value of $r_0$ at which this maximum occurs, i.e.

$$\left.\frac{\partial g(r_0, x)}{\partial r_0}\right|_{r_0=r_f} = 0. \tag{52}$$

The gas hold-up $\alpha_g$ (49) is singular at $r_f$. This implies that the local bubble volume fraction will be high, however small $\alpha_0$ may be. At such locations, bubble interactions should no longer be neglected. Care is required when integrating the volume flux of bubbles $q_g$ (46) across the singularity at $r_0 = r_f$.

There is a similar problem at the axis. If bubbles from a region $r_0 < r < r_0 + \delta r_0$ at $x_0$ pass through a region $0 < r < \delta r_1$ on the axis at $x$, there will be an infinite (but integrable) volume fraction of bubbles on the axis. This corresponds to $g(r_0, x) = r_1 = 0$ in the denominator of Eq. (49). Fig. 12 shows $rP(x, r)$ (which by Eq. (49) is well behaved at $r = 0$) at various axial positions $x$ along the pipe.

Once both the convected volume flux $q_g$ (46) and the lost volume flow $q_g^{lost}$ (51) have been computed, we may check the conservation of bubble volume flux along the pipe. Errors were smaller than 1% at all points investigated.

Another way to indicate the distribution of bubble volume fraction across the cross-section of the pipe, while avoiding the visual confusion of integrable singularities, is to compute the cumulative contribution to gas hold-up from the axis out to a radius $r < R_p$ as a function of $r$. Thus, we may define

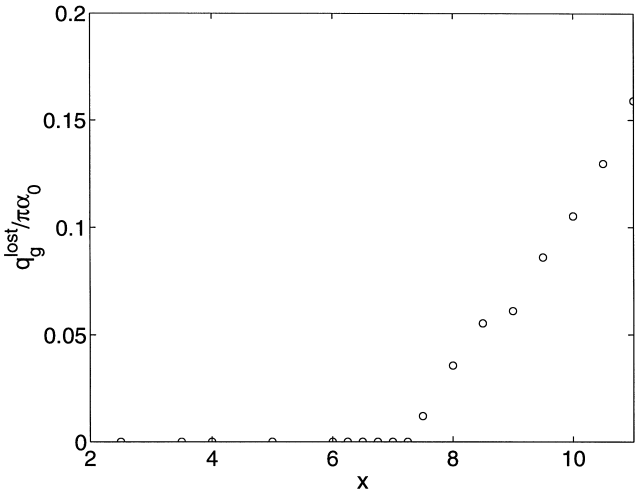


Fig. 11. Fraction of bubbles which have hit the pipe wall, as a function of the axial position $x$.

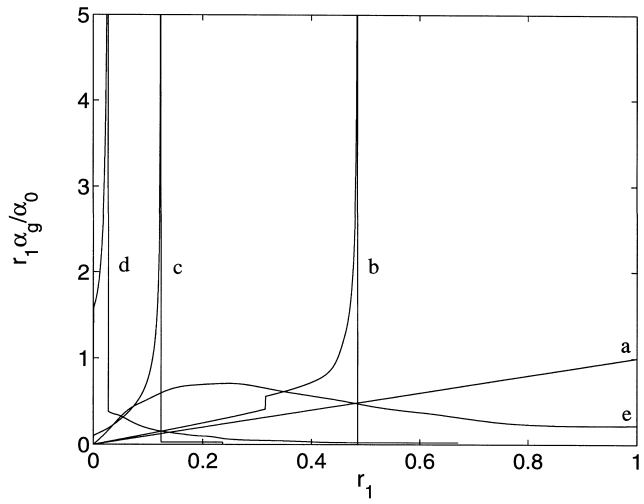


Fig. 12. Gas volume fraction $\alpha_g$ scaled by $\alpha_0$ and multiplied by $r_1$, as a function of radial position $r_1$. (a) $x = 2.5$; (b) $x = 4$; (c) $x = 6$; (d) $x = 8$; (e) $x = 11$.

$$\alpha_g^P(x, r) = \frac{2}{R_p^2}\int_0^r r_1\alpha_g(x, r_1)\,dr_1. \tag{53}$$

Fig. 13 shows $\alpha_g^P/\alpha_0$ as a function of $r$, at various axial positions $x$ along the pipe. Note that in some cases $\alpha_g^P$ increases (albeit slowly) with $r$ when $r > g(r_f)$. This is due to the presence of bubbles which originated on the far side of the axis and which have subsequently migrated across almost the entire width of the pipe. Conservation of volume requires that the gas

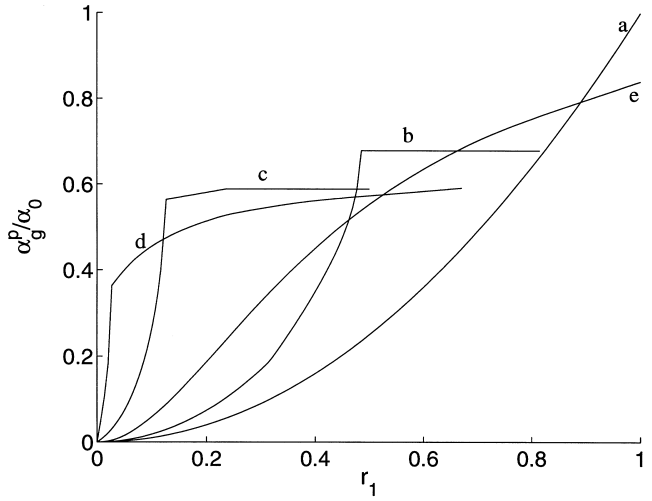


Fig. 13. Integrated gas volume fraction $\alpha^P$ defined by Eq. (53). (a) $x = 2.5$; (b) $x = 4$; (c) $x = 6$; (d) $x = 8$; (e) $x = 11$.

volume fraction $\alpha_g$ decreases within the throat, where bubbles travel faster than the liquid, and so $\alpha_g^P(x, R_p) \leq 1$ even when no bubbles have hit the walls of the pipe.

Similarly, we define the partial flux of bubbles $q_g^P$ over a cross section of radius $r$:

$$q_g^P(x, r) = \int_0^r r_1 \alpha_g(x, r_1) v_x(x, r_1)\, dr_1. \tag{54}$$

Fig. 14 shows $q_g^P/\pi\alpha_0$ as a function of $r$, for various values of axial position $x$. Note that when $x > 7.3$ the flux $q_g = q_g^P(x, R_p) < 1$, since some bubbles have already hit the walls.

## 5. The effect of drag on bubble trajectories in potential flow

### 5.1. The effect of drag on trajectories on the axis

When the bubble is on the axis, numerical solutions of the full one-dimensional equation (21), using the potential flow velocity, predict oscillations for $0.061 \leq M_d \leq 2.84$. This may be compared to the oscillation range $0.056 \leq M_d \leq 2.92$ found in Section 3.2 assuming that the liquid velocity $u_l$ (20) is uniform over the pipe cross-section. We see from Fig. 6 that the velocity at the pipe wall differs from that along the centreline only at the sharp corners of the pipe. The uniform velocity (20) is therefore a good approximation to the centre-line velocity for potential flow. Fig. 15 shows the position of the bubble as a function of time when $M_d = 0.115$, together with the shape of the Venturi. Note that the bubble velocity reverses at $x = 11$, somewhat downstream of the end of the diverging section $x_4 = 10.5$. As seen in Fig. 6, the potential flow velocity does not immediately become uniform downstream of the diverging section. Fig. 16 shows the bubble velocity corresponding to the results of Fig. 15. Note that the

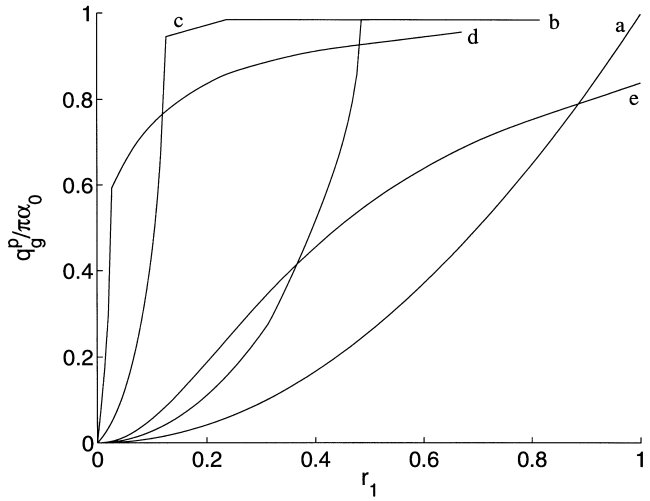


Fig. 14. Integrated gas volume flow rate $q_g^P$ defined by Eq. (54) at various axial positions $x$. (a) $x = 2.5$; (b) $x = 4$; (c) $x = 6$; (d) $x = 8$; (e) $x = 11$.

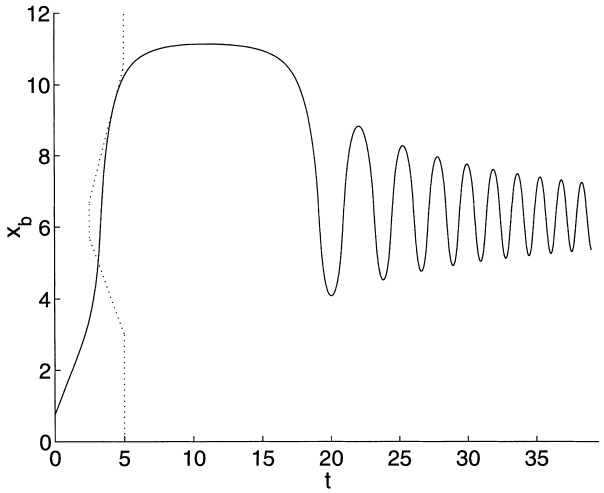


Fig. 15. The position $x_b$ of the bubble as a function of time $t$, computed using the potential flow velocity along the centreline. $M_d = 0.115$. The dotted line indicates the shape of the Venturi.

oscillation is now much closer to the simple harmonic motion predicted in Section 3.3 for a smooth velocity profile than to the asymmetric oscillations (Fig. 4) predicted with the one-dimensional liquid velocity (20).

### 5.2. The effect of drag on trajectories off the axis

In Section 4, we computed the trajectories of bubbles in a Venturi in the absence of drag, using the potential flow velocity field. We now repeat these computations and include drag.

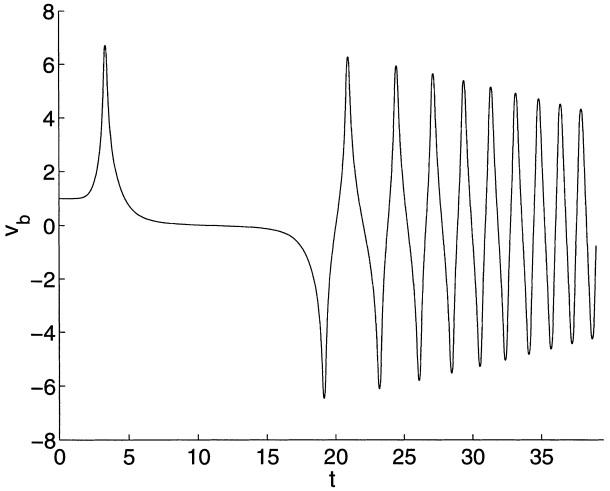


Fig. 16. The velocity $v_b$ of the bubble in Fig. 15.

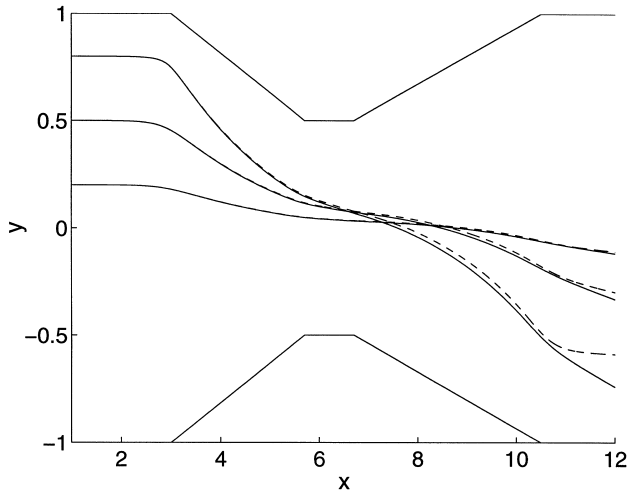


Fig. 17. Bubble trajectories: ——— $M_d = 0$ (no drag); - - - - - with drag $M_d = 0.036$.

Fig. 17 shows trajectories without drag. When a small amount of drag ($M_d = 0.036$) is introduced, the trajectories change only slightly.

If drag is increased, the results of Section 5.1 indicate that oscillations will occur on the centre-line. Off the centre-line, the axial velocity of the bubble reverses, as seen in Fig. 18 for $M_d = 1$ and 2. However, the bubbles have a non-zero radial velocity. They move towards the walls and, in particular, towards the low pressure (high liquid velocity) regions near the corners at the start and end of the throat. Computations were stopped once the bubbles reach the wall, and the oscillations do not survive for long.

If drag is increased further, the bubbles are carried through the Venturi by the liquid and

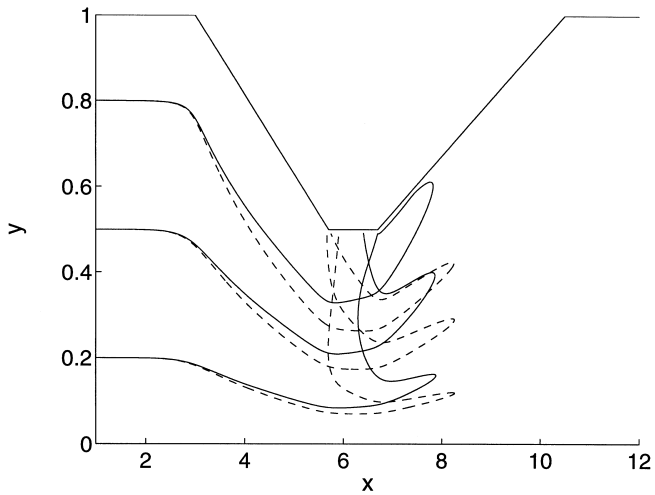


Fig. 18. Bubble trajectories: ——— $M_d = 2$; - - - - - $M_d = 1$.

oscillations cease. The greater $M_d$ becomes, the closer the bubbles follow the liquid streamlines (which have fore-aft symmetry), as seen in Fig. 19.

In Section 2, the strain lift force $\boldsymbol{F}_{ls}$ was discussed. Although this force is small compared to the pressure and added mass forces, it is not clear that it is reasonable to neglect $\boldsymbol{F}_{ls}$ while allowing a drag force $\boldsymbol{F}_d$ to act. If we assume that strain rates typically have magnitude $U/a$, so that non-dimensional strain rates are $O(1)$, then lift is large compared to drag if $M_{ls} \gg M_d$, i.e. if

$$Re \gg \frac{2^{1/2}|\boldsymbol{u}_l - \boldsymbol{v}_b|^{1/2}}{R_0^{5/2}}\left(\frac{18}{4.8}\right)^{3/2} \approx \frac{10|\boldsymbol{u}_l - \boldsymbol{v}_b|^{1/2}}{R_0^{5/2}}, \tag{55}$$

where the non-dimensional velocity difference $|\boldsymbol{u}_l - \boldsymbol{v}_b|$ is $O(1)$ (or more precisely $O(\beta^{-2})$ within the throat), or smaller if drag is large. The inertial forces are much greater than the lift forces if $M_a \gg M_{ls}|\boldsymbol{u}_l - \boldsymbol{v}_b|$ i.e. if

$$Re \gg \left(\frac{4.8}{3}\right)^3 \frac{|\boldsymbol{u}_l - \boldsymbol{v}_b|^2}{2R_0} \approx \frac{2|\boldsymbol{u}_l - \boldsymbol{v}_b|^2}{R_0}. \tag{56}$$

Since $R_0 \ll 1$, this simple order of magnitude estimate suggests that the lift forces will only be larger than drag when the Reynolds number $Re$ is sufficiently large such that both lift and drag are negligible. If lift is larger than drag because $|\boldsymbol{u}_l - \boldsymbol{v}_b|$ is small, then both lift and drag can be neglected compared to inertial forces. However, this argument must be treated with care. Strain rates are larger than $O(U/a)$ in the neighbourhood of the corners at the start and end of the throat, and lift forces are not collinear with drag. Fig. 20 shows trajectories with $M_d = 3.6$ and $M_{ls}|\boldsymbol{u}_l - \boldsymbol{v}_b|^{1/3} = 0.48$, corresponding to $\tilde{R}_0 = 0.5$ mm, $\tilde{a} = 5$ cm, $\tilde{U} = 1$ m s$^{-1}$, $\tilde{\rho}_l = 10^3$ kg m$^{-3}$, and $\tilde{\mu} = 10^{-3}$ Pa s. Trajectories computed without lift differ from those with lift, but the difference is small and can be seen only within the throat. A bubble which oscillates (or

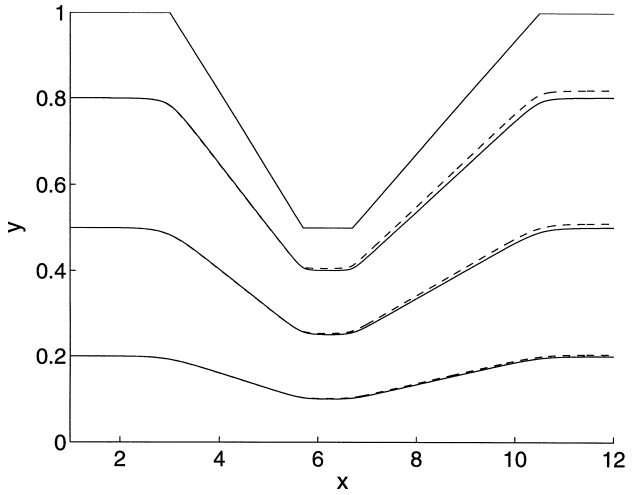


Fig. 19. Bubble trajectories: - - - - - $M_d = 180$; ——— $M_d = 1800$.

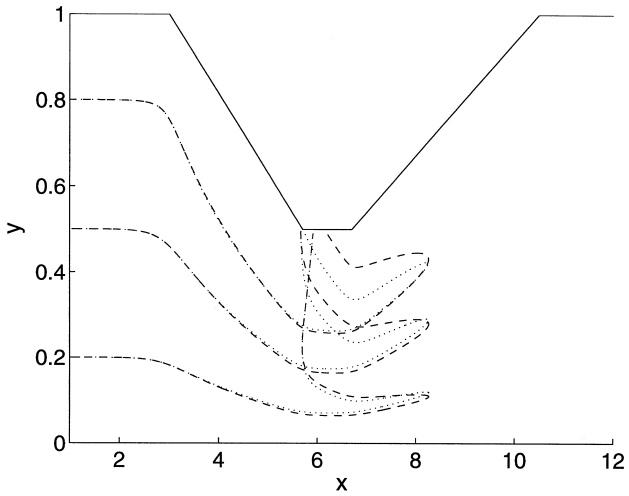


Fig. 20. Bubble trajectories, $M_d = 3.6$. - - - - - with lift force $M_{ls}|\boldsymbol{u}_l - \boldsymbol{v}_b|^{1/3} = 0.48$; · · ·· · · without lift force ($M_{ls} = 0$).

attempts to do so) moves slowly in the throat, and this allows the lift force to act for a sufficiently long time to have a noticeable effect. In practice, if the bubble is no longer spherical, the lift coefficient will no longer be given by Eq. (12).

## 6. Concluding remarks

The oscillations described in Sections 3.2 and 5.1 have not (to our knowledge) been observed. As discussed in Section 3.4, one possible explanation is the likely deformation (and breakup) of bubbles within the Venturi due to high Weber numbers. The Levich drag (20) is unlikely to be appropriate: indeed, if oscillations occurred it is possible that any steady drag law would be inappropriate. Moreover, if a fluid with exceptionally high interfacial tension were found (so that bubbles remain spherical), it is clear from the computations of Section 5.2 that any perturbation away from the centreline would quickly cause bubbles to move to the walls of the Venturi.

Simple models of two-phase flow through a Venturi make various assumptions concerning the amount of mechanical coupling, via interaction forces, between the gas and liquid. One extreme assumption is that of complete separation, in which gas and liquid independently satisfy Bernoulli's equation and flow at quite different velocities. Another extreme case is that in which slip between the liquid and gas is assumed to be zero, and the pressure drop is that due to a homogeneous fluid with the mean mixture density. Predictions of the pressure drop within a Venturi for these two cases differ, and it is therefore important to understand the degree of radial separation of the two phases.

## References


Auton, T.T., Hunt, J.C.R., Prud'homme, M., 1988. The force exerted on a body in inviscid unsteady non-uniform rotational flow. J. Fluid Mech. 197, 241–257.

Batchelor, G.K., 1973. An Introduction to Fluid Dynamics. Cambridge University Press, Cambridge.

Boyer, C., Lemonnier, H., 1996. Design of a flow metering process for two-phase dispersed flows. Int. J. Multiphase Flow 22, 713–732.

British Standards Institution, 1997. BS EN ISO 5167-1 Measurement of fluid flow by means of pressure differential devices, British Standards Institution, London.

Cai, X., Wallis, G.B., 1992. Potential flow around a row of spheres in a circular tube. Phys. Fluids A 4, 904–912.

Clift, R., Grace, J.R., Weber, M.E., 1978. Bubbles, Drops and Particles. Academic Press, New York.

Climent, E., Magnaudet, J., 1997. Simulation d'écoulements induits par des bulles dans un liquide initialement au repos. C.R. Acad. Sci. Paris 324, Ser. IIb, 91–98.

Hunt, J.C.R., Perkins, R.J., Fung, J.C.H., 1997. Review of the problems of modelling disperse two-phase flows. Multiphase Science and Technology 8, 595–643.

Jaswon, M.A., Symm, G.T., 1977. Integral Equation Methods in Potential Theory and Elastostatics. Academic Press, New York.

Johnson Jr., V.E., Hsieh, T., 1966. The influence of the trajectories of gas nuclei on cavitation inception. In: Proc. 6th ONR Symp. on Naval Hydrodynamics, 163–182.

Kim, H.S., Prosperetti, A., 1992. Numerical simulation of the motion of rigid spheres in potential flow. SIAM J. Appl. Math 52, 1533–1562.

Kowe, R., Hunt, J.C.R., Hunt, A., Couet, B., Bradbury, L.J.S., 1988. The effects of bubbles on the volume fluxes and the pressure gradients in unsteady and non-uniform flow of liquids. Int. J. Multiphase Flow 14, 587–606.

Kuo, J.T., Wallis, G.B., 1988. Flow of bubbles through nozzles. Int. J. Multiphase Flow 14, 547–564.

Lance, M., Lopez de Bertodano, M., 1994. Phase distribution phenomena. Multiphase Science and Technology 8, 69–123.

Lopez de Bertodano, M., Lahey, R.T., Jones, O.C., 1994. Phase distribution in bubbly two-phase flow in vertical ducts. Int. J. Multiphase Flow 20, 805–818.

Magnaudet, J., Legendre, D., 1998. Some aspects of the lift force on a spherical bubble. Appl. Sci. Res 58, 441–461.

Moore, D.W., 1965. The velocity of rise of distorted gas bubbles in a liquid of small viscosity. J. Fluid Mech 23, 749–766.

Muir, J.F., Eichorn, R., 1963. Compressible flow of an air–water mixture through a vertical, two-dimensional, converging–diverging nozzle. In: Proc. 1963 Heat transfer and Fluid Mechanics. Inst., Stanford University Press.

Oldenziel, D.M., 1979. Bubble cavitation in relation to liquid quality, Ph.D. thesis, Tech. Univ. Twente, Delft Hydraulics Laboratory Publ. no. 211.

Serizawa, A., Kataoka, I., 1994. Dispersed flow. Multiphase Science and Technology 8, 125–194.

Sherwood, J.D., 2000. Potential flow around a deforming bubble in a Venturi, Int. J. Multiphase Flow, in press.

Smythe, W.R., 1961. Flow around a sphere in a circular tube. Phys. Fluids 4, 756–759.

Thang, N.T., Davis, M.R., 1979. The structure of bubbly flow through Venturis. Int. J. Multiphase Flow 5, 17–37.

Thorn, R., Johansen, G.A., Hammer, E.A., 1997. Recent developments in three-phase flow measurement. Meas. Sci. Technol 8, 691–701.

Tsao, H.K., Koch, D.L., 1997. Observations of high Reynolds number bubbles interacting with a rigid wall. Phys. Fluids 9, 44–56.

van Wijngaarden, L., 1972. One-dimensional flow of liquids containing small gas bubbles. Ann. Rev. Fluid Mech 4, 369–396.